IEEE Access
Multidisciplinary ⋮ Rapid Review ⋮ Open Access Journal

Received October 5, 2020, accepted November 23, 2020, date of publication November 26, 2020,
date of current version December 11, 2020.

Digital Object Identifier 10.1109/ACCESS.2020.3040898

Bessel Beam Generation Using Dielectric Planar Lenses at Millimeter Frequencies

ÁLVARO F. VAQUERO[1], (Student Member, IEEE), MARCOS RODRIGUEZ PINO[1], MANUEL ARREBOLA[1], (Senior Member, IEEE), SÉRGIO A. MATOS[2,3], (Senior Member, IEEE), JORGE R. COSTA[2,3], (Senior Member, IEEE), AND CARLOS A. FERNANDES[2], (Senior Member, IEEE)

[1]Group of Signal Theory and Communications, Department of Electrical Engineering, University of Oviedo, 33202 Gijón, Spain
[2]Instituto de Telecomunicações, Instituto Superior Técnico, Universidade de Lisboa, 1049-001 Lisbon, Portugal
[3]Departamento de Ciências e Tecnologias da Informação, Instituto Universitário de Lisboa (ISCTE-IUL), 1649-026 Lisbon, Portugal

Corresponding author: Álvaro F. Vaquero (fernandezvalvaro@uniovi.es)

This work was supported in part by the Ministerio de Ciencia, Innovación y Universidades under Project TEC2017-86619-R (ARTEINE), in part by Gobierno del Principado de Asturias and Fondo Europeo de Desarrollo Regional (FEDER) under Project GRUPIN-IDI/2018/000191, and in part by the COST (European Cooperation in Science and Technology) under COST Action TD1301, MiMed.

ABSTRACT In this work a dielectric planar lens is proposed to generate a Bessel beam. The lens works at Ka-band and produces a non-diffraction range within the Fresnel region of the antenna. The methodology to design the aperture antenna at millimetre or microwave frequencies is presented. It is applied to a dielectric planar lens made up of cells that shapes the radiated near-field by adjusting the unit cell response. An approach based on a second order polynomial is proposed to consider the angular dependence of the phase-shift response of the cell in the designing process. In order to implement the lens physically, two novel cells, based on rectangular and hexagonal prisms, are proposed, and their performance is compared. The cells ensure the index dielectric media variation using airgaps to control the overall density of the material. After fully characterizing the cells, a design is carried out for the two proposed type of cells. The requirement for the Bessel beam is a depth-of-field of 650 mm at 28 GHz. After evaluating the design in a full-wave simulation, both prototypes were manufactured using a 3-D printing technique. Finally, the prototypes were measured in a planar acquisition range to evaluate the performances of the Bessel beam. Both lenses show a good agreement between simulations and measurements, obtaining promising results in the Bessel beam generation by index-graded dielectric lenses at Ka-band.

INDEX TERMS Dielectric lenses, Bessel beams, near-field focusing.

I. INTRODUCTION

Near-field applications have increased their popularity throughout last years. Most of these applications require antennas that concentrate the radiated power on a certain area, typically within their Fresnel region, the radiated near-field zone. Traditionally, near-field focusing antennas have been particularly useful in applications such as RFID [1], [2], wireless power transfer (WPT) [3] or medical applications [4]. However, other applications such as near-field radars for industrial inspection [5] or detection [6], imaging [7], communications [8] or material characterization [9] demand antennas whose radiated power is not only focused on a point but on a finite area, increasing the tolerance in the probe positioning. A desirable solution for these applications is a near-field focusing beam without diffraction through its near-field region, thus its transversal profile on the propagation direction remains unaltered within a significant range.

Non-diffraction beam solutions have been widely used in many applications at high frequency bands, particularly at optical bands, where different techniques have been developed [10]–[12]. Recently, several works have studied new techniques to generate non-diffraction beams at lower bands, making the best efforts at millimeter-wave and microwave bands. A common approach is the design of antennas whose fields at the aperture are similar to a Bessel function. These solutions are typically achieved using radial slot arrays (RLSA) [13]–[15], near-field plates [16] or leaky radial waveguides [17], [18], among others. An alternative is the

The associate editor coordinating the review of this manuscript and approving it for publication was Necmi Biyikli.

use of structures that transform an incident wave to a non-diffraction beam, such as axicons [19], [20], holograms [21] or meta-surfaces [22]. A new approach is the use of a phase shifting surface (PSS) [23] or transmitarrays [9] to generate near-fields with a large depth-of-field at Ka and V bands, respectively.

Although these previous works obtain good performances creating non-diffraction beams, they have some drawbacks. The generation of Bessel beam functions at the antenna aperture typically require a complex design or manufacturing process. On the other hand, structures like axicons or holograms involve high costs, complex manufacturing process and bulky solutions. However, planar antenna apertures (transmitarrays, lenses, PSS ...) minimize these issues, being a suitable alternative in the generation of non-diffraction beams at millimeter band. In this line, graded-index dielectric lenses could be considered as a potential candidate to create these beams too. The working principle of these antennas is similar to a PSS or transmitarrays but the introduced phase-shift of the incoming wave is controlled by the variation of the index dielectric media of the cell. One main advantage regards on the easiness and low-cost fabrication process due to the use of 3-D printing technology [24]–[26]. This process is typically applied to planar lenses, where the index dielectric variation is obtained by adjusting the height of the cells to obtain the desired phase-shift [27]. However, this technique does not provide a planar profile in both surfaces therefore, diffraction problems may appear owing to the edge of the cells on the non-planar surface.

In this paper, a graded-index only dielectric lens is proposed to generate a near-field with a large depth-of-field, particularly a Bessel beam, at Ka-band. Two novel cells, based on square and hexagonal prims respectively, are proposed to physically implement the lens. Both cells are characterized, and two designs are carried out to evaluate their overall performances. The designed lenses are manufactured using a 3-D printing technique and measured on a planar acquisition range. The measured near field shows a good agreement with simulations.

II. FUNDAMENTALS OF BESSEL BEAMS IN FINITE APERTURES

The main characteristic of Bessel beams is the constant intensity of the field along the propagation distance [28]. Ideal Bessel beams are generated by infinite apertures or apertures whose size is thousands of λ. The amplitude of an ideal Bessel beam is given by

$$E(\rho, z) = E_0 e^{-jk_z z} J_0(k_\rho \rho) \tag{1}$$

where J_0 is the zero-order Bessel function, k_ρ and k_z are the radial and longitudinal components of the free space wave vector, such that $k_0^2 = k_\rho^2 + k_z^2$.

However, regarding finite apertures, pseudo Bessel beams are produced. Unlike ideal Bessel beams, the amplitude of the pseudo Bessel beams only remains constant on a certain propagation distance before spreading rapidly. The beam is produced by the generation of a near-field interference pattern that basically keeps constant within an area. The size of this area is given by the size of the antenna aperture D.

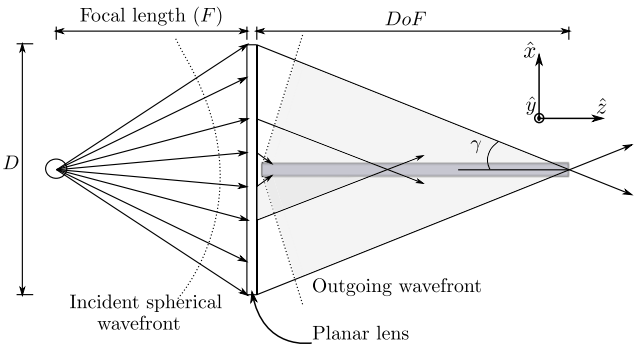

FIGURE 1. Sketch of the Bessel beam generation through finite aperture antennas using near-field interferences.

When this concept is applied at millimeter frequencies and, particularly to planar lenses, the working principle is based on the transformation of a spherical incoming wavefront to a plane wave with wave vector lying on a cone, as Fig. 1 depicts. The outgoing wave front must generate a near-field interference pattern that behaves as a pseudo Bessel beam. As Fig. 1 shows, the extent of the shadowed area is defined by D and γ, and it is called depth-of-field (DoF). The DoF can be computed using (2) and it also defines the theoretical 3 dB contour of the field.

$$DoF = \frac{D/2}{\tan(\gamma)} \tag{2}$$

Theoretically, the maximum distance achievable is limited by the Fresnel region of the antenna ($2D^2/\lambda$). Regarding the angle γ, it must satisfy $\sin(\gamma) \ll 1$, otherwise the scalar Bessel beam theory, previously explained, cannot be applied [29].

Let us consider a planar lens comprised by a given number of elements regularly distributed on a $N_x \times N_y$ grid. The lens feed is located at a focal length F to generate a Bessel beam with angle γ. According to Fig. 1, the outgoing wave front must have its wave vector laying on a cone as long as the wave front is radiated through the propagation direction $\hat{z}$. This condition allows to create the required near-field interference pattern to generate the desired beam.

Then, the phase-shift of the lens elements can be computed using geometrical optics. The phase produced by the elements of the lens are given by

$$\varphi_{lens}(\rho) = -\varphi_{inc}(\rho) - \varphi_{wf} - \frac{2\pi}{\lambda}\rho \tan \gamma \tag{3}$$

where φ_{wf} is the phase of the outgoing wave front; ρ is the axial position of an element computed as $\rho = \sqrt{x_m^2 + y_n^2}$, considering the center of the lens the center of the circumference; and $\varphi_{inc}(\rho)$ is the incident phase at an element defined by

$$\varphi_{inc}(\rho) = -\frac{2\pi}{\lambda}\sqrt{F^2 + \rho^2} \tag{4}$$

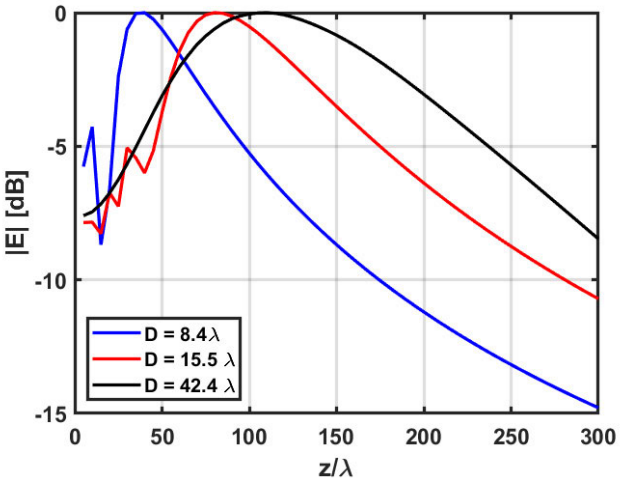

FIGURE 2. Comparison of Bessel beams using different aperture sizes assuming ideal lens elements computed with (2) and $F = 150$ mm and $\gamma = 5°$ with a $\cos^q$ feed ($q = 7$).

Fig. 2 shows a comparison of Bessel lenses axial intensities for different aperture sizes while keeping γ and F constant. As expected, the use of larger apertures generates beams more similar to ideal Bessel beams with a constant intensity on the propagation direction.

III. DIELECTRIC LENS ELEMENTS

A. WORKING PRINCIPLE OF DIELECTRIC CELLS

A planar lens is required to have the same height in every cell. One approach that satisfy this condition is using total dielectric cells. These cells behave as an effective index media that adds a certain delay to the transmitted ray. The effective index media η_{eff} is related to the effective dielectric constant as $n^2_{eff}(\rho) = \epsilon_{eff}(\rho)$. Thus, the variation of ϵ_{eff} allows to physically implement the phase-shift $\phi_{lens}(\rho)$ of the cell.

Let us assume two spatially uniform and isotropic materials with dielectric constants ϵ_1 and ϵ_2, respectively. If the second material is embedded in the other, the effective dielectric constant of the assembled cell does not depend on the geometry but on the dielectric constants and its volume fraction [30]–[32]. The effective dielectric constant of the cell can be computed as

$$\epsilon_{eff} = \epsilon_1 \frac{2\epsilon_1 + \epsilon_2 + 2P(\epsilon_2 - \epsilon_1)}{2\epsilon_1 + \epsilon_2 - P(\epsilon_2 - \epsilon_1)} \tag{5}$$

where P is the volume fraction of the material ϵ_2 over the total volume of the cell. If one of the dielectrics is air, only one dielectric is needed to accomplish (5), being $\epsilon_2 = \epsilon_0$.

In this work, the proposed cells are based on polylactic acid (PLA) ($\epsilon_1 = 2.85$ and $\tan\delta = 0.0121$@40 GHz) [33] used as the host material and air ($\epsilon_2 = 1$) to perform the inclusions. Two different cells are analyzed, particularly, square and hexagonal prism cells. In both cases, a variable airgap is embedded in the cell to change the volume fraction and control the $\phi_{lens}(r)$ that is introduced.

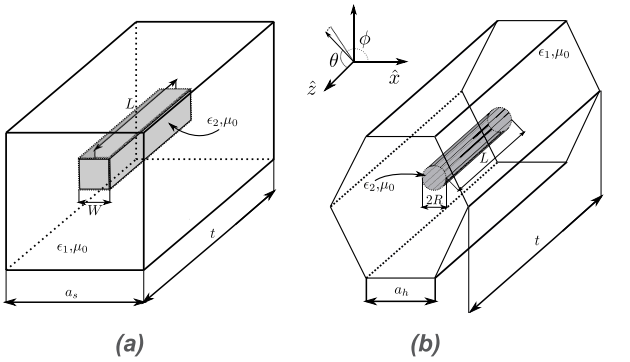

FIGURE 3. Sketch of dielectric cells based on airgaps insertions to control the effective dielectric constant of the total cell. (a) Square prism airgaps (b) Cylindrical airgaps.

B. PHASE RESPONSE WITH AIRGAPS

The square prism cells, Fig. 3(a), are based on a square PLA prism of dimensions $a \times a \times t$, and a second embedded airgap prism of variable dimensions $W \times W \times L$ as Fig. 3 shows. The variation of these dimensions changes the volume of air, therefore P:

$$P = \frac{V_{airgap}}{V_{prism}} = \frac{W^2 \times L}{a^2 \times t} \tag{6}$$

The cell is analyzed with CST Microwave Studio [34] using periodic boundary conditions in x- and y-axis and open in z-direction. The cell is illuminated by a normal plane wave propagating in the z-direction with the electric field defines in the y-direction. The dimensions of the PLA prism are $\lambda_d/2 \times \lambda_d/2 \times 2\lambda_d(a_s \times a_s \times t)$, whilst the embedded prism dimensions are swept between $W \in (0, \lambda_d/2)$ and $L \in [0, 2\lambda_d]$. So, either full dielectric cells ($\epsilon_{eff} = 2.85$) or almost air cells ($\epsilon_{eff} = 1.28$) are considered. The analysis is performed at central frequency of 28 GHz in a bandwidth of 2 GHz, and λ_d is computed as λ_0 at the highest frequency, 30 GHz.

The amplitude and phase response of the transmission coefficient of the cell as function of the airgap dimensions are shown in Fig. 4, at the central frequency and normal incidence. The different combinations of L and W totally cover the 360° required range to implement $\varphi_{lens}(\rho)$. More than 85% of the cells present transmission losses lower than 1.5 dB. These values are expected since the $\tan\delta$ of PLA is significantly high. Additionally, Fig. 5 shows the relation between the dimensions of the airgap and the effective dielectric constant of each cell.

On the other hand, the hexagonal cells, Fig. 3 (b), use an embedded cylinder airgap. In accordance with (4), this change in the geometries does not affect the phase-shift so long as P is the same as the square prism cells. Consequently, the volume of the airgaps, both cylinder and square prism, must be the same and the volume of the square and hexagonal prism are also equal. Considering that the lens depth is independent from the type of selected cell, equals to

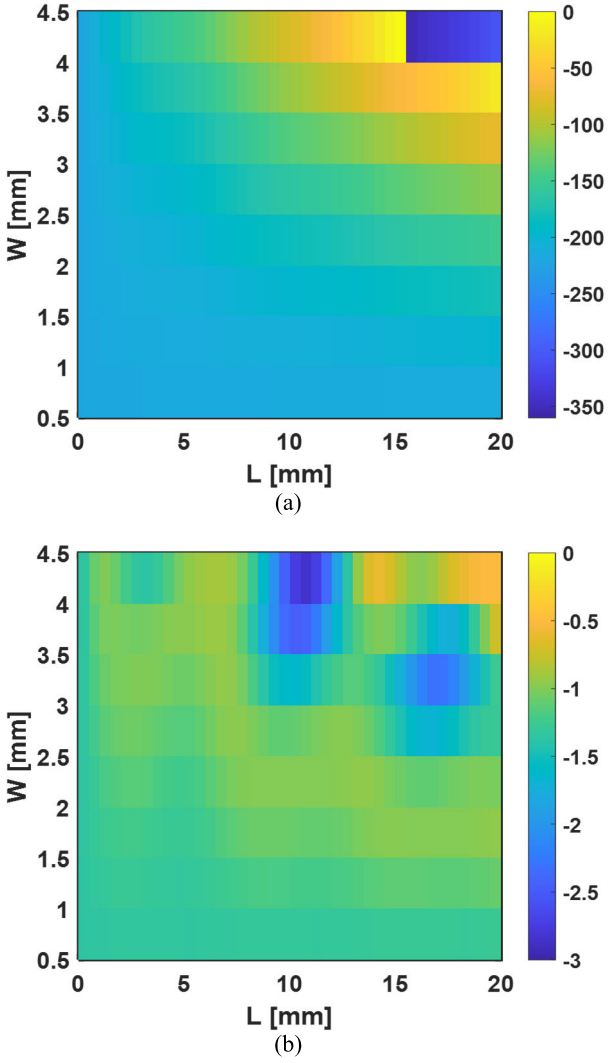

FIGURE 4. Square prism cell response in function of the airgap dimensions for normal incident at 28 GHz. (a) Phase (deg) (b) Amplitude (dB).

$t = 2\lambda_d$, the condition is only imposed on the cell prism base. Therefore, a hexagon of radius $a_h = 0.31\lambda_d$ is obtained.

In order to compute the cylinder dimensions, the depth of the cylinders remain alike to the depth of square prism airgaps, L. Thus, only the radius needs to be calculated using $R^2 = W^2/(\pi)$. In Fig. 6, the amplitude and phase of the transmission coefficient versus frequency for different square and hexagonal prisms are compared, showing that the geometry does not affect the cell response.

C. ANGULAR PERFORMANCES

The phase stability of the cell has been analyzed for different angles of incidence θ and ϕ at 28 GHz. It was considered linear polarization of the incident electric field and angles with variation in $\phi = 0°, 45°$ and $90°$ and $\theta \in [0, 30]°$, being $\theta = 0°$ normal incidence. Fig. 7 shows the phase responses from a set of 6 different cells as a function of

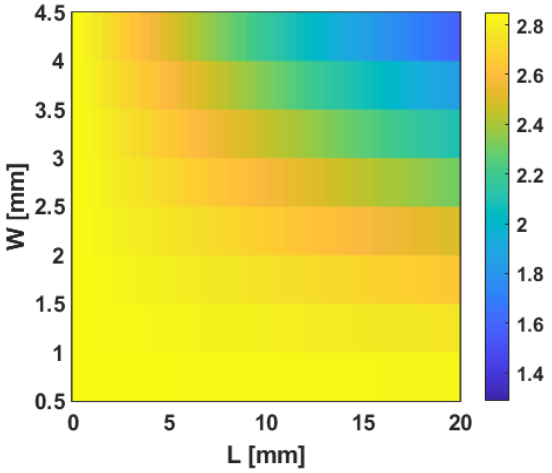

FIGURE 5. Effective dielectric constant of the square prism cell regarding the volume fraction of air and PLA.

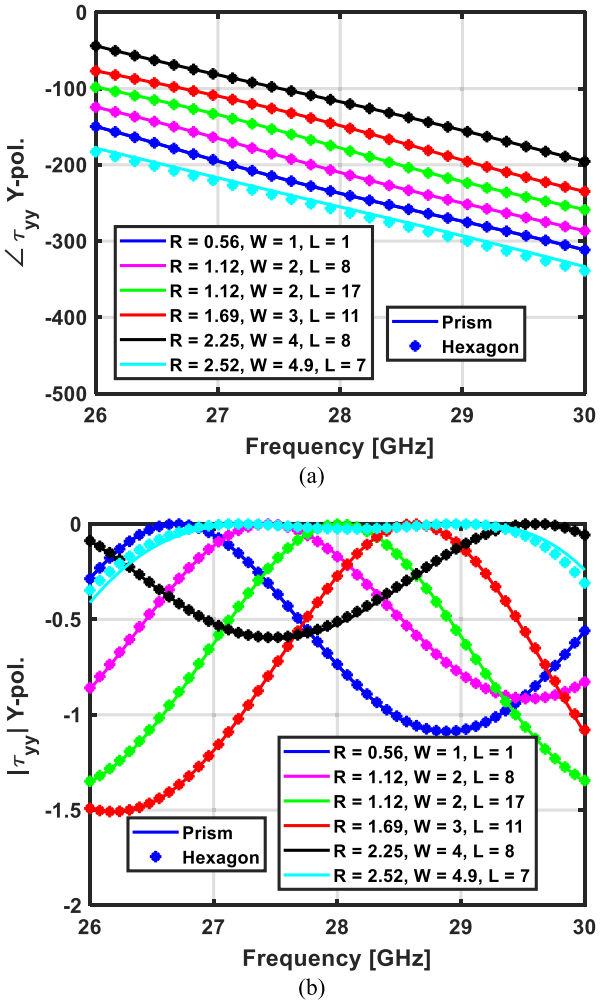

FIGURE 6. Comparison of the (a) transmission phase and (b) transmission amplitude of the different prisms with the same filling factor. Airgap dimensions are in mm.

θ and ϕ. These results show the independence to ϕ, whilst θ notably modifies the phase-shift regarding normal incidence. The dependence of phase-shift versus θ can be approximated

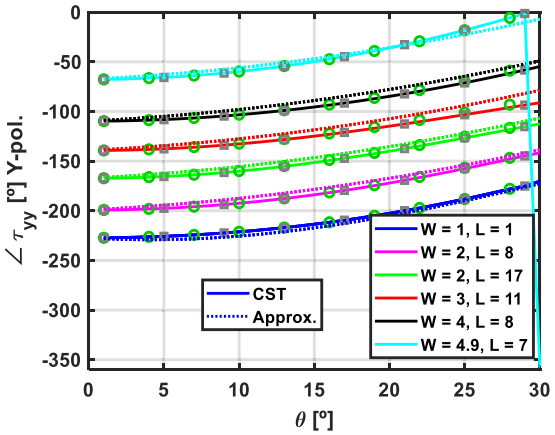

FIGURE 7. Phase response analyzed for different angles of incidence and the approximation obtained by a polynomial expression for different cells at 28 GHz. (solid) $\phi = 0°$ (Grey square) $\phi = 45°$ (Green circle) $\phi = 90°$. Airgap dimensions are in mm.

by a second-order polynomial as:

$$\Delta\varphi\,(\theta) = p_1 \cdot \theta + p_2 \cdot \theta^2 \tag{7}$$

As shown in Fig. 7, the curve shape is very similar to the analyzed cells and the polynomic model of $\Delta\varphi$ in the previous equation is common for all of them ($p_1 = 0.7453$ and $p_2 = 0.0425$). Then, the phase of the transmission coefficient for each cell of the lens can, therefore, be determined using the following equation.

$$\varphi_{lens}\,(\theta) = \varphi_{norm} + \Delta\varphi(\theta) \tag{8}$$

being $\Delta\varphi$ obtained with the polynomial (6) and φ_{norm} the phase of the transmission coefficient obtained for normal incidence analysis. This function nearly predicts the real phase-shift of a cell under oblique incidence, without considering the angle on the preliminary cell study. The maximum error produced in most cases is lower than 5°.

IV. DIELECTRIC BESSEL LENS BASED ON AIRGAP CELLS

In order to validate both square and hexagonal prism cells, this section addresses the lens design and simulation for both type of cells.

A. ANTENNA OPTICS

The proposed antenna to generate a Bessel beam is a square planar dielectric lens of equivalent aperture D of 120×120 mm^2 at 28 GHz. The distribution of the elements depends on the cell geometry. For square cells, a regular grid is used with periodicity 5×5 mm^2 and made up of 24×24 elements. In the case of the hexagonal prism cells, they are arranged as a honeycomb, so the cells are located on an axial distribution as shown in Fig. 8.

The lenses are defined using a centered optics (see Fig. 1), and the phase center of the feed is placed at $(x_f, y_f, z_f) = (0, 0, F = -100)$ mm, taking the center of the lens as the origin of the system of coordinates.

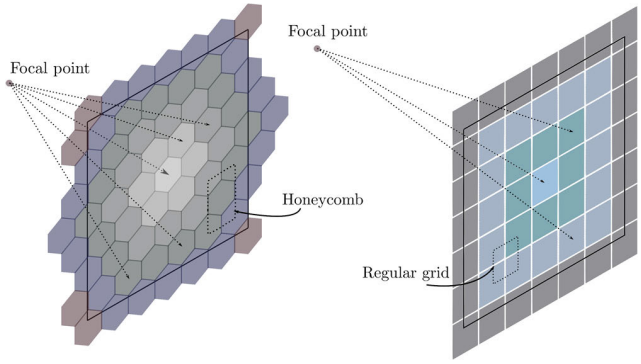

FIGURE 8. Cell distribution of the lens elements (left) Hexagon prism cells (right) Square prism cell.

The proposed antenna should generate the Bessel beam close to the lens, therefore a maximum DoF of 650 mm is established. According to (2), the beam theoretically behaves as a Bessel beam within this area if $\gamma = 5°$.

B. DESIGN PROCEDURE

The lens design is based on geometrical optics theory according to (3) and (4). These equations provide the required phase-shift that should introduce the lens elements to radiate the beam previously defined. In this case, the phase distribution of the elements along the lens surface is shown in Fig. 9, reminding the physical distribution shown in Fig. 8.

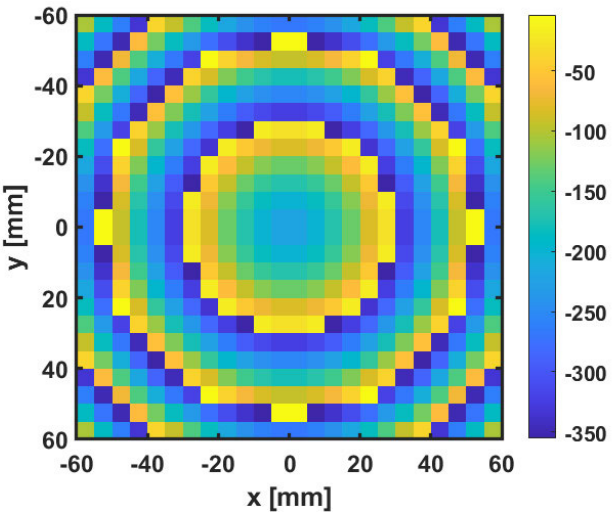

FIGURE 9. Transmission phase-shift (deg) of the lens element along the surface to generate the desired Bessel beam.

Once the phase distribution along the lens surface is computed, the elements must be designed. In the designing process, the dimensions of the airgaps (R, W and L) are adjusted to produce the required phase-shift according to $\phi_{lens}(\rho)$ in equation (3). Note that for, each cell, the incidence angle (θ), the focal distance (F) of the lens and the radius of the center

of the cell in the lens (ρ) are related through

$$\theta = \text{atan}\left(\frac{\rho}{F}\right) \tag{9}$$

Therefore, the equation (6) can be rewritten in the following form:

$$\Delta\varphi\,(\rho) = p_1 \cdot \text{atan}\left(\frac{\rho}{F}\right) + p_2\left(\text{atan}\left(\frac{\rho}{F}\right)\right)^2 \tag{10}$$

And then substituting (10) in (8)

$$\varphi_{lens}\,(\rho) = \varphi_{norm} + \Delta\varphi\,(\rho) = \varphi_{norm} + p_1 \cdot \text{atan}\left(\frac{\rho}{F}\right) + p_2\left(\text{atan}\left(\frac{\rho}{F}\right)\right)^2 \tag{11}$$

Finally, the adjustment is done element by element, considering the real angle of incidence φ_{norm} shown in Fig. 4(b) with the desired one $\varphi_{lens}(\rho)$ of Fig. 9. In order to improve the design, an angular correction $\Delta\varphi(\rho)$ is introduced throughout the process; thus, the real phase-shift of each cell is considered. The resulting lens layout is made by the cells that minimize their phase-shift to the theoretical response. The amplitude of the cell response is used to discard cells with high losses.

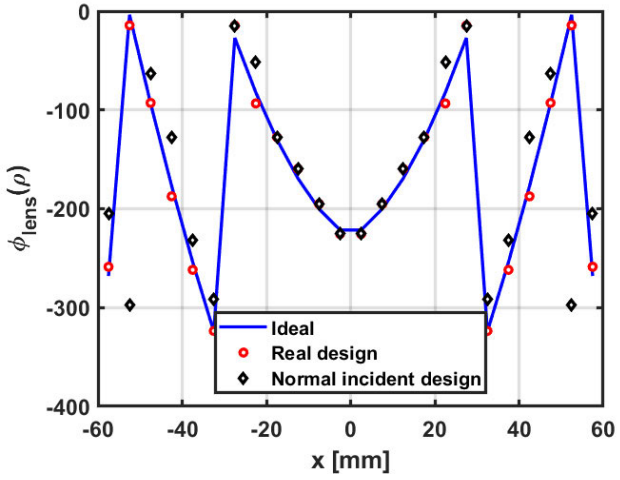

FIGURE 10. Cut $y = 0$ mm of the phase-shift (deg) of the lens element along the lens surface to generate the desired Bessel beam.

In Fig. 10 the cut $y = 0$ mm of the theoretical phase distribution is compared with the chosen cell of the final design, showing a good agreement between both. Additionally, a comparison with the design, based only on normal incidence, is done to highlight the importance of the angular correction through the design process. Notice that the difference between selected cells occurs more at the edge of the lens where the incidence angle is farther from the normal incidence. Two different layouts are obtained, one for each type of cell.

In the evaluation of the Bessel beam performances, both layouts have been analysed with CST Microwave Studio [32] in a full-wave simulation (see Fig. 11). The selected feed is a pyramidal horn antenna with 15 dBi gain placed at a distance $F = 100$ mm from the surface of the lens.

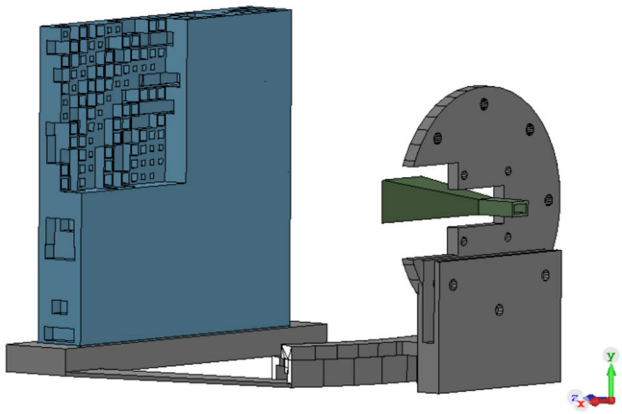

FIGURE 11. Depicted setup of the full-wave simulation carried out in CST Microwave Studio. A half quarter of the lens has been removed to observe the airgap inclusions.

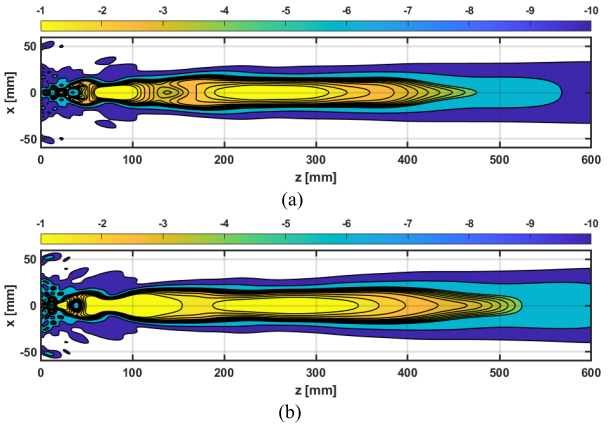

FIGURE 12. *XoZ* plane of the Bessel beam created by the lens using (a) square prism cells (b) hexagonal prism cells.

This configuration illuminates the lens surface with an amplitude taper of -17 dB at the edge of the lens.

The simulation results are shown in Fig. 12 for the *XoZ* plane and in Fig. 14 the electric field along the z-axis is compared with the measurements. Because the horn antenna is non-symmetric regarding its main cuts, E- and H- plane, the outgoing wave-front is not perfectly formed. Hence, the near-field interference pattern is not properly created in the closest area of the antenna, having strong fluctuations on this area. This effect is minimized when hexagonal prism cells are used in the design. The cells achieve a more stable beam and concentrate it through a larger range than square prism cells, as Fig. 12 shows. However, when a horn antenna feeds a Bessel beam generator with small aperture, it is expected to obtain a shorter DoF range than the one computed with (2).

V. EXPERIMENTAL RESULTS

Both planar dielectric lenses, made up of either square or hexagonal cells, have been manufactured and evaluated in the planar acquisition range at University of Oviedo. The lenses have been manufactured using a Fused Deposition Modeling (FDM), a 3-D printing technique based on the melting

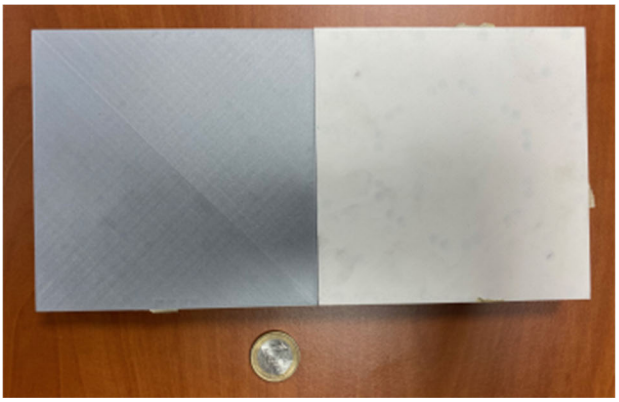

(a)

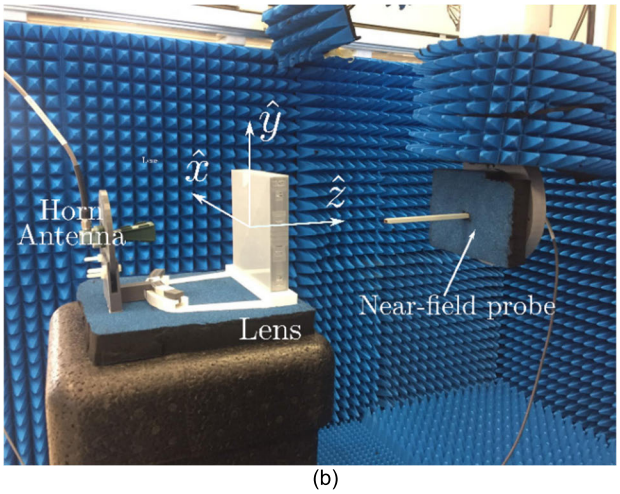

(b)

FIGURE 13. (a) Manufactured prototypes using 3-D printing techniques (FDM). Lens made up of hexagon prism cells (left) and lens made up of square prism cells (right). (b) Setup at the planar acquisition range of University of Oviedo to measure the planar dielectric lens of hexagon prism cells at Ka-band.

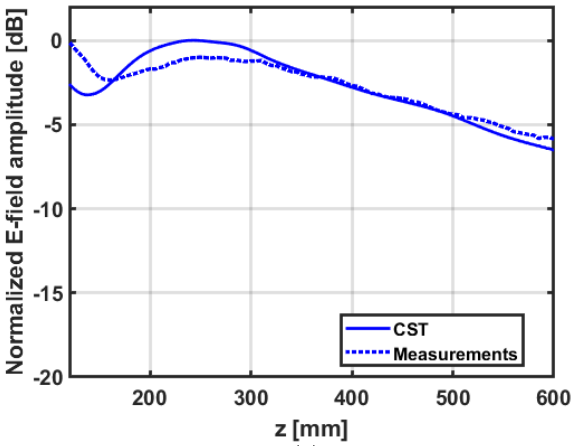

(a)

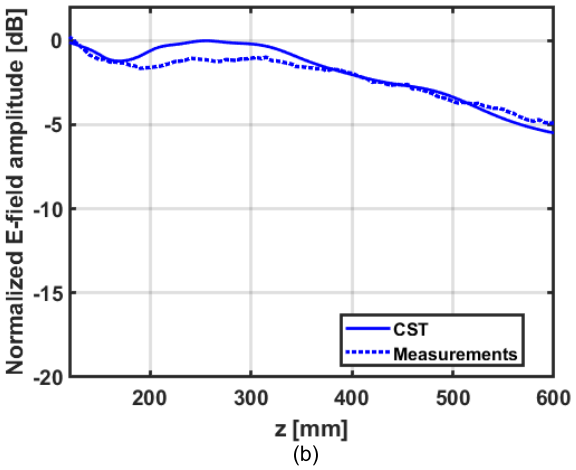

(b)

FIGURE 14. Comparison between simulations and measurements of the normalized amplitude (dB) of the electric field along z-direction and $x = y = 0$ at 28 GHz. (a) Square prism cell lens (b) hexagonal prism cell lens.

and extrusion of a thermoplastic polymer, such PLA, through a nozzle tip to deposit the material layer-by-layer onto a platform. This technique is widely used in additive manufacturing processes to fabricate prototypes since its easily controlled and reduces the costs significantly. However, when dealing with accurate designs likes these lenses, it is important to set a proper configuration to obtain a high precision. Especially, the thickness wall and layer height since both control the resolution of the pieces. In this case, the thickness wall is set to 0.4 mm and the layer height to 0.1 mm, providing a high-resolution printing. Low resolution configuration could modify or eliminate the internal wall of low infill cell (P factor close to 1), therefore change the effective dielectric constant and the cell response. On the other hand, high-resolution configurations inherently increase the printing time to 40 hours for the lens made of square prism cells and 48 hours for the lens made of hexagon prisms cells. Throughout the whole process is highly relevant to keep the environmental conditions, for instance variation on temperature could produce air flows and lead to structural deformations on the pieces such as curvatures on the corners.

Both prototypes are shown in Fig. 13(a) and Fig. 13(b) depicts the setup used to measure both lenses. In this setup a vector network analyzer (PNA-X of Keysight) is connected to the feeding horn, a pyramidal standard gain horn of 15 dBi gain, whilst the second port is connected to the probe, an open-ended Ka-band waveguide. The lens is placed on a PLA structure aligned to the aperture of the probe. The measurements are performed from 26 to 30 GHz evaluating the electric field at the horizontal plane XoZ and at different transversal planes XY.

The normalized electric field along the propagation direction $\hat{z}$ is compared with simulations in Fig. 14 at 28 GHz. Measurements highly agreed with simulations, highlighting the range of the DoF or the decay of the Bessel beam. Additionally, the transversal $XoZ(y = 0)$ plane is shown in Fig. 15 at different frequencies for both lenses. The 3 dB level indicates the maximum attenuation allowed in the DoF, whose theoretical range is 650 mm according to (2). Both lenses obtain their best results at the highest frequencies, from 28 to 30 GHz, where the DoF reaches

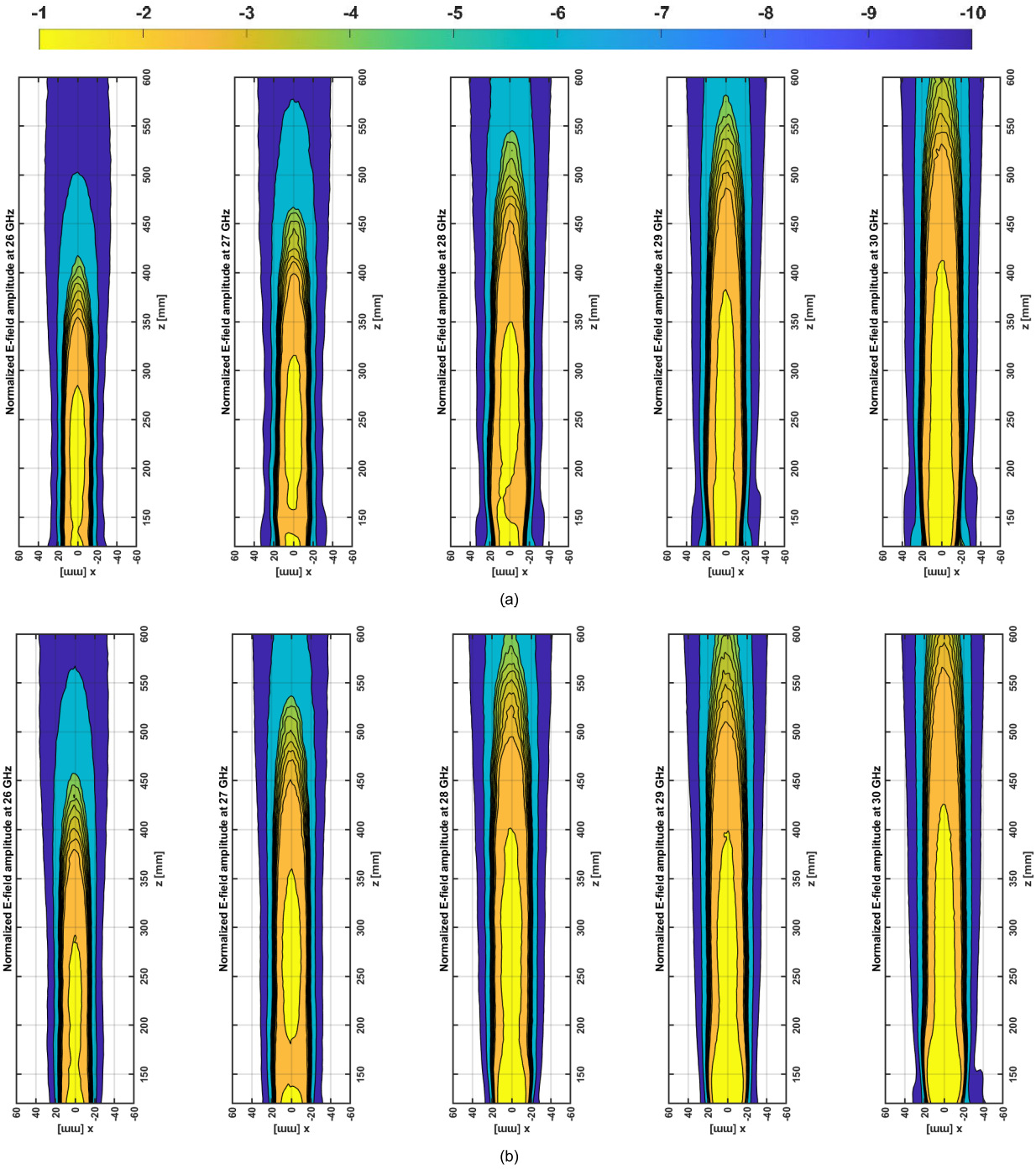

FIGURE 15. Normalized measured amplitude (dB) of the (a) square cell (b) hexagon cell lens at different frequencies at the plane *xoz* ($y = 0$).

a 475 ($47.50\lambda_0$) mm range. It is worth noting the hexagonal prism lens behavior, showing an improvement in the results regarding the square prism cell. The in-band response, particularly at the upper frequencies, barely change, whilst square prism lens increases its variation due to frequency shifts. Furthermore, the non-diffraction area is larger in all cases, but it also starts closer to the antenna aperture, creating a more stable Bessel beam through the propagation direction.

The transverse profile is also evaluated in a plane XY at $z = 250$ mm at 26.5, 28 and 29.5 GHz. The plane is parallel to the antenna aperture and shown in Fig. 16. Measurements show good axial symmetry with a field distribution similar to the Bessel main lobe, whilst the side lobes are hidden due to the antenna size.

The cut $y = 0$ of three different transversal XY planes, $z = 150$, 200 and 250 mm, is measured at the whole band and

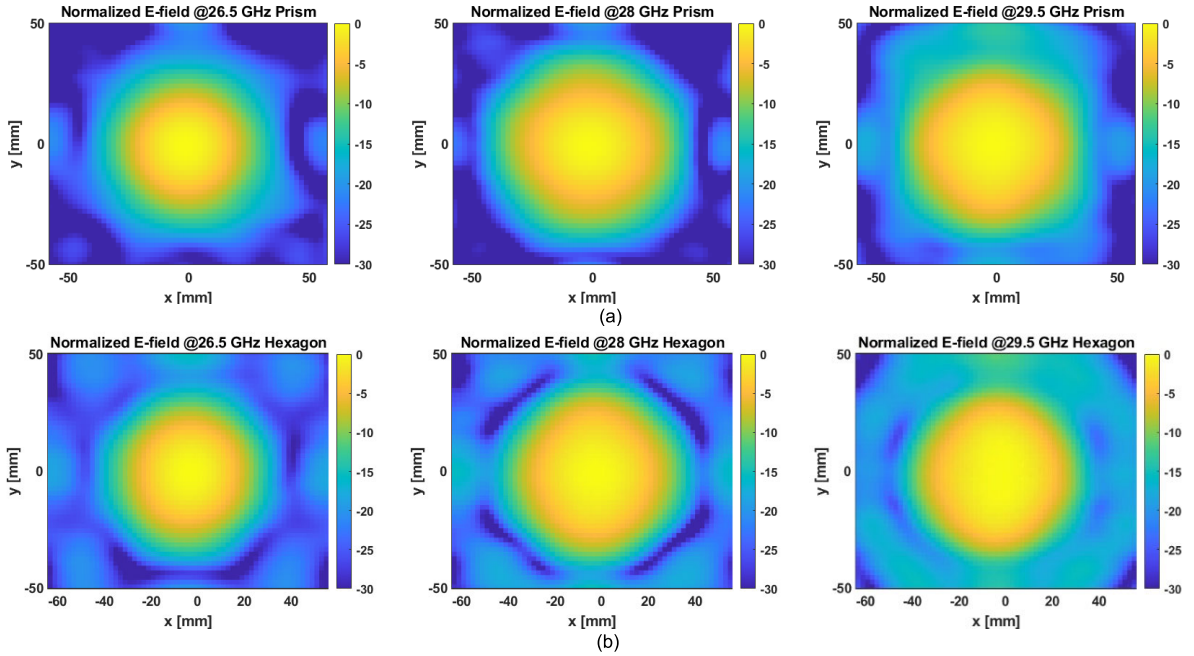

FIGURE 16. Measured transversal *XY* profiles at $z = 250$ mm parallel to the antenna aperture at 26.5, 28 and 29.5 GHz.

TABLE 1. Comparison of the antenna and Bessel beam performances with published works.

Ref.	Frequency [GHz]	Size [λ_0(@GHz)]	Thickness [λ_0(@GHz)]	Phase-shift implementation	Depth-of-field [λ_0(@GHz)]	Manufacturing technique
[24]	35	(14×14) (35)	1.51(35)	Height of the cell	23.33(35)	NA
[25]*	60	13.12(60)	1.16(60)	Height of the cell	30.00(60)	Simulation results
[26]	$26 - 32$	20(30)	2.00(30)	Height of the cell	11.13(26)14.90(29) 18.13(32)	NA
[36]	300	15(300)	1.90(300)	Height of the cell	11.00(300)	In-home developed technique using laser and high-temperature resin
[35]	300	15(300)	2.02(300)	Height of the cell	11.20(300)	Stereo Lithography (SLA)
This work	$26 - 30$	$(12 \times 12)(30)$	2.00(30)	Airgaps insertions	21.40(26) (square prism) 24.00(26) (hexagon prism) 32.85(28) (square prism) 38.73(28) (hexagon prism) 43.70(30) (square prism) 47.50(30) (hexagon prism)	Fused Deposition Modeling (FDM)

*This work presents a 3-D printed axicon lens based on dielectric cells instead of a planar lens.

shown in Fig. 17. These measurements evaluate the beam-waist of the beams through the non-diffraction range. Neither the hexagonal prism lens nor the square prism lens is able to properly form the beam at the closest plane, $z = 150$ mm. However, at $z = 200$ mm the beam of the hexagonal prism lens is similar to a Bessel distribution and the beam is confined in a spot smaller than 4λ. The main lobe of the square prism lens is flattened at this plane, especially at 28 GHz and higher frequencies. At the further plane, $z = 250$ mm, the square prism lens shows a beam similar to a Bessel function. As expected, the hexagonal prism lens keeps its Bessel behaviour. It must be noted that the hexagonal beam-waist nearly unchanges when the frequency varies.

Different published works of 3-D printed Bessel lens are compared in Table 1. Regardless the geometry and frequency, these works use cells based on a height variation to control the phase-shift introduced by each cell. In this work, the cell keeps its height constant and the phase-shift is obtained by the insertions of airgaps, obtaining a double planar surface lens that minimizes possible diffractions caused by the height difference of the cells and offers an easier integration of the lens. Considering the size, the depth-of-field and, especially

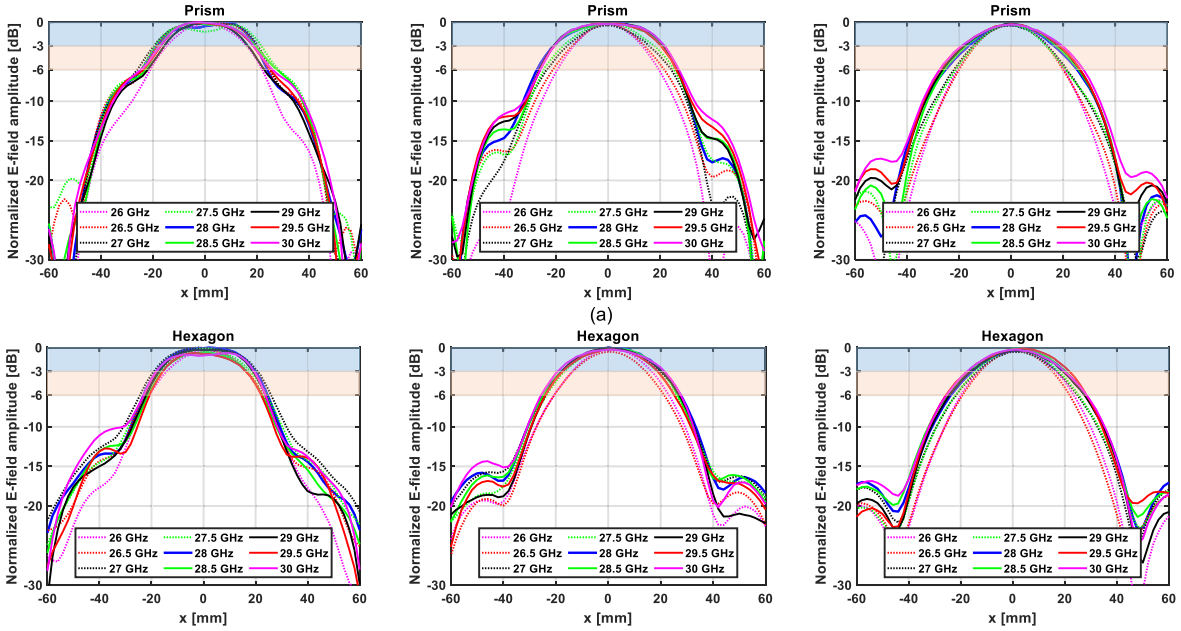

FIGURE 17. Normalized amplitude (dB) at (left) $z = 150$ mm (center) $z = 200$ mm and (right) $z = 250$ mm and $y = 0$ and different frequencies.

working in Ka-band, the results of this work make the proposed cells as an attractive solution in the generation of Bessel beams using 3-D printing technology in millimeter band.

VI. CONCLUSION

Dielectric planar lenses are demonstrated to generate near-field Bessel beams in Ka-band. The proposed lenses are made up of dielectric cells based on either square or hexagonal prisms. Both cells ensure the variation of their index dielectric media using airgaps to control the overall density of the material. A design is carried out to generate a Bessel beam with a depth-of-field of 650 mm, and it has been implemented for both type of cells, each one based on a proposed cell. The dependence of the phase response of the cell and the angle of incidence is considered with a second order polynomial. Both prototypes were manufactured using a 3-D printing technique and measured in a planar acquisition range, obtaining a good agreement between simulations and measurements. Although measurements show good performances in both cases, the hexagonal prism cell exhibits a superior behavior regarding the non-diffraction range and the in-band response. In light of these results, graded-index dielectric lenses have demonstrated to be a potential candidate to generate Bessel beams at Ka-band frequencies, taking the advantage of reducing the manufacturing cost process and reaching a simple structure.

REFERENCES

[1] A. Buffi, A. A. Serra, P. Nepa, H.-T. Chou, and G. Manara, "A focused planar microstrip array for 2.4 GHz RFID readers," *IEEE Trans. Antennas Propag.*, vol. 58, no. 5, pp. 1536–1544, May 2010.

[2] H.-T. Chou, T.-M. Hung, N.-N. Wang, H.-H. Chou, C. Tung, and P. Nepa, "Design of a near-field focused reflectarray antenna for 2.4 GHz RFID reader applications," *IEEE Trans. Antennas Propag.*, vol. 59, no. 3, pp. 1013–1018, Mar. 2011.

[3] Y. Li and V. Jandhyala, "Design of retrodirective antenna arrays for short-range wireless power transmission," *IEEE Trans. Antennas Propag.*, vol. 60, no. 1, pp. 206–211, Jan. 2012.

[4] K. D. Stephan, J. B. Mead, D. M. Pozar, L. Wang, and J. A. Pearce, "A near field focused microstrip array for a radiometric temperature sensor," *IEEE Trans. Antennas Propag.*, vol. 55, no. 4, pp. 1199–1203, Apr. 2007.

[5] D. Oloumi and K. Rambabu, "Metal-cased oil well inspection using near-field UWB radar imaging," *IEEE Trans. Geosci. Remote Sens.*, vol. 56, no. 10, pp. 5884–5892, Oct. 2018.

[6] D. A. Hill, "Near-field detection of buried dielectric objects," *IEEE Trans. Geosci. Remote Sens.*, vol. 27, no. 4, pp. 364–368, Jul. 1989.

[7] J. M. Felicio, J. M. Bioucas-Dias, J. R. Costa, and C. A. Fernandes, "Antenna design and near-field characterization for medical microwave imaging applications," *IEEE Trans. Antennas Propag.*, vol. 67, no. 7, pp. 4811–4824, Jul. 2019.

[8] A. F. Vaquero, D. R. Prado, M. Arrebola, and M. R. Prado, "Reflectarray antennas for 5-G indoor coverage," in *Proc. 13th Eur. Conf. Antennas Propag. (EuCAP)*, Krakow, Poland, Apr. 2019, pp. 1–4.

[9] L. Dussopt, K. Medrar, and L. Marnat, "Millimeter-wave Gaussian-beam transmitarray antennas for quasi-optical *S*-parameter characterization," *IEEE Trans. Antennas Propag.*, vol. 68, no. 2, pp. 850–858, Feb. 2020.

[10] J. Durnin, "Exact solutions for nondiffracting beams. I. The scalar theory," *J. Opt. Soc. Amer. A, Opt. Image Sci.*, vol. 4, no. 4, pp. 651–654, 1987.

[11] J. Durnin, J. J. Miceli, and J. H. Eberly, "Diffraction-free beams," *Phys. Rev. Lett.*, vol. 58, pp. 1499–1501, Apr. 1987.

[12] D. McGloin and K. Dholakia, "Bessel beams: Diffraction in a new light," *Contemp. Phys.*, vol. 46, no. 1, pp. 15–28, Jan. 2005.

[13] M. Ettorre, S. C. Pavone, M. Casaletti, and M. Albani, "Experimental validation of Bessel beam generation using an inward hankel aperture distribution," *IEEE Trans. Antennas Propag.*, vol. 63, no. 6, pp. 2539–2544, Jun. 2015.

[14] D. Comite, G. Valerio, M. Albani, A. Galli, M. Casaletti, and M. Ettorre, "Exciting vorticity through higher order Bessel beams with a radial-line slot-array antenna," *IEEE Trans. Antennas Propag.*, vol. 65, no. 4, pp. 2123–2128, Apr. 2017.

[15] M. Albani and S. C. Pavone, "Optimization of a RLSA Bessel beam launcher for a microwaves near-field link," in *Proc. Int. Conf. Electromagn. Adv. Appl. (ICEAA)*, Granada, Spain, Sep. 2019, p. 1329.

[16] M. F. Imani and A. Grbic, "Generating evanescent Bessel beams using near-field plates," *IEEE Trans. Antennas Propag.*, vol. 60, no. 7, pp. 3155–3164, Jul. 2012.

[17] W. Fuscaldo, G. Valerio, A. Galli, R. Sauleau, A. Grbic, and M. Ettorre, "Higher-order leaky-mode Bessel-beam launcher," *IEEE Trans. Antennas Propag.*, vol. 64, no. 3, pp. 904–913, Mar. 2016.
[18] M. Ettorre, S. M. Rudolph, and A. Grbic, "Generation of propagating Bessel beams using leaky-wave modes: Experimental validation," *IEEE Trans. Antennas Propag.*, vol. 60, no. 6, pp. 2645–2653, Jun. 2012.
[19] J. Arlt and K. Dholakia, "Generation of high-order Bessel beams by use of an axicon," *Opt. Commun.*, vol. 177, nos. 1–6, pp. 297–301, Apr. 2000.
[20] Y. Z. Yu and W. B. Dou, "Production of THz pseudo-Bessel beams with uniform axial intensity using irregular binary axicons," *IET Optoelectron.*, vol. 4, no. 5, pp. 195–200, Oct. 2010.
[21] A. Vasara, J. Turunen, and A. T. Friberg, "Realization of general nondiffracting beams with computer-generated holograms," *J. Opt. Soc. Amer. A, Opt. Image Sci.*, vol. 6, no. 11, p. 1748, Nov. 1989.
[22] M. Qing Qi, W. X. Tang, and T. J. Cui, "A broadband Bessel beam launcher using metamaterial lens," *Sci. Rep.*, vol. 5, no. 1, p. 11732, Dec. 2015.
[23] Y. C. Zhong and Y. J. Cheng, "Ka-band wideband large depth-of-field beam generation through a phase shifting surface antenna," *IEEE Trans. Antennas Propag.*, vol. 64, no. 12, pp. 5038–5045, Dec. 2016.
[24] Y. Gan, H. Meng, Y. Chen, X. Zhang, and W. Dou, "Generation of Bessel beams with 3D-printed lens," *Int. J. RF Microw. Comput. Aided Eng.*, vol. 30, no. 4, Nov. 2019, Art. no. e22029.
[25] P.-Y. Feng and S.-W. Qu, "Generation of Bessel beams at millimeter-wave band using 3-D printed axicon lenses," in *Proc. Int. Symp. Antennas Propag. (ISAP)*. Busan, South Korea, Oct. 2018, pp. 1–2.
[26] Y. L. Fan, X. Q. Lin, and S. L. Liu, "Ka-band quasi-nondiffraction beam generation through a broadband Bessel lens antenna," in *Proc. IEEE Asia–Pacific Microw. Conf. (APMC)*, Dec. 2019, pp. 1223–1225.
[27] H. Yi, S.-W. Qu, K.-B. Ng, C. H. Chan, and X. Bai, "3-D printed millimeter-wave and terahertz lenses with fixed and frequency scanned beam," *IEEE Trans. Antennas Propag.*, vol. 64, no. 2, pp. 442–449, Feb. 2016.
[28] S. Monk, J. Arlt, D. A. Robertson, J. Courtial, and M. J. Padgett, "The generation of Bessel beams at millimetre-wave frequencies by use of an axicon," *Opt. Commun.*, vol. 170, nos. 4–6, pp. 213–215, Nov. 1999.
[29] S. R. Mishra, "A vector wave analysis of a Bessel beam," *Opt. Commun.*, vol. 85, nos. 2–3, pp. 159–161, Sep. 1991.
[30] J. C. M. Garnett, "Colors in metal glasses and in metallic films," *Phil. Trans. Roy. Soc. A*, vol. 23, nos. 359–371, pp. 385–420, Jan. 1904.
[31] B. Sareni, L. Krähenbühl, A. Beroual, and C. Brosseau, "Effective dielectric constant of periodic composite materials," *J. Appl. Phys.*, vol. 80, no. 3, pp. 1688–1696, Aug. 1996.
[32] A. H. Sihvola and J. A. Kong, "Effective permittivity of dielectric mixtures," *IEEE Trans. Geosci. Remote Sens.*, vol. 26, no. 4, pp. 420–429, Jul. 1988.
[33] J. M. Felicio, C. A. Fernandes, and J. R. Costa, "Complex permittivity and anisotropy measurement of 3D-printed PLA at microwaves and millimeter-waves," in *Proc. 22nd Int. Conf. Appl. Electromagn. Commun. (ICECOM)*, Dubrovnik, Croatia, Sep. 2016, pp. 1–6.
[34] CST Microwave Studio. (Oct. 2017). *Computer Simulation Technology*. [Online]. Available: http://www.cst.com
[35] G.-B. Wu, K. F. Chan, W. C. Mok, and C. H. Chan, "3-D printed terahertz lens for Bessel beam generation," in *Proc. IEEE Asia–Pacific Microw. Conf. (APMC)*, Singapore, Dec. 2019, pp. 637–639.
[36] G.-B. Wu, K. F. Chan, S.-W. Qu, and C. H. Chan, "A 2-D beam-scanning Bessel launcher for terahertz applications," *IEEE Trans. Antennas Propag.*, vol. 68, no. 8, pp. 5893–5903, Aug. 2020.

ÁLVARO F. VAQUERO (Student Member, IEEE) was born in Salinas, Spain, in 1990. He received the B.Sc. and M.Sc. degrees in telecommunications engineering from the Universidad de Oviedo, Gijón, Spain, in 2015 and 2017, respectively, where he is currently pursuing the Ph.D. degree.

Since 2016, he has been a Research Assistant with the Group of Signal Theory and Communications, University of Oviedo. In 2017, he was with the Instituto de Telecomunicações, Lisbon, Portugal, where he was involved in broadband planar lenses for skin cancer imaging. His current research interests include the development of efficient techniques for the analysis and synthesis of reflectarrays and planar lenses and the design of 3-D printed lenses for near-field applications.

MARCOS RODRIGUEZ PINO was born in Vigo, Spain, in 1972. He received the M.Sc. and Ph.D. degrees in telecommunication engineering from the University of Vigo, Vigo, in 1997 and 2000, respectively.

In 1998, he was a Visiting Scholar with the ElectroScience Laboratory, The Ohio State University, Columbus, OH, USA. From 2000 to 2001, he was an Assistant Professor with the University of Vigo. Since 2001, he has been with the Electrical Engineering Department, University of Oviedo, Gijón, Spain, where he is currently an Associate Professor, teaching courses on communication systems and antenna design. His current research interests include antenna design, measurement techniques, and efficient computational techniques applied to EM problems, such as evaluation of radar cross section or scattering from rough surfaces.

MANUEL ARREBOLA (Senior Member, IEEE) was born in Lucena (Córdoba), Spain. He received the M.Sc. degree in telecommunication engineering from the University of Málaga, Málaga, Spain, in 2002, and the Ph.D. degree from the Technical University of Madrid (UPM), Madrid, Spain, in 2008.

From 2003 to 2007, he was a Research Assistant with the Electromagnetism and Circuit Theory Department, UPM. In 2005, he was a Visiting Scholar with the Microwave Techniques Department, Universität Ulm, Ulm, Germany. In 2007, he joined the Electrical Engineering Department, University of Oviedo, Gijón, Spain, where he is currently an Associate Professor. In 2009, he enjoyed a two-month stay at the European Space Research and Technology Centre, European Space Agency, Noordwijk, The Netherlands. In 2018, he was a Visiting Professor with the Edward S. Rogers Sr. Department of Electrical and Computer Engineering, University of Toronto, Toronto, ON, Canada. In 2019, he was a Visiting Professor with the Institute of Sensors, Signals and Systems, Heriot-Watt University, Edinburgh, U.K. His current research interests include the development of efficient analysis, design, and optimization techniques of reflectarray and transtmitarray antennas both in near and far fields.

Dr. Arrebola was a co-recipient of the 2007 S. A. Schelkunoff Transactions Prize Paper Award by the IEEE Antennas and Propagation Society.

SÉRGIO A. MATOS (Senior Member, IEEE) received the Licenciado, M.Sc., and Ph.D. degrees in electrical and computer engineering from the Instituto Superior Técnico (IST), University of Lisbon, Lisbon, Portugal, in 2004, 2005, and 2010, respectively.

He is currently a Researcher with the Instituto de Telecomunicações (IT), Lisbon. He is also an Assistant Professor with the Departamento de Ciências e Tecnologias da Informação, Instituto Universitário de Lisboa (ISCTE-IUL). He has coauthored 80 technical papers in international journals and conference proceedings. His current research interests include electromagnetic wave propagation in metamaterials, flat-lens design, and transmit arrays.

JORGE R. COSTA (Senior Member, IEEE) was born in Lisbon, Portugal, in 1974. He received the Licenciado and Ph.D. degrees in electrical and computer engineering from the Instituto Superior Técnico (IST), Technical University of Lisbon, Lisbon, in 1997 and 2002, respectively.

He is currently a Senior Researcher with the Instituto de Telecomunicações, Lisbon. He is also a Full Professor with the Departamento de Ciências e Tecnologias da Informação, Instituto Universitário de Lisboa (ISCTE-IUL). His current research interests include lenses, transmit-arrays, and biomedical antennas. He is the coauthor of four patent applications and more than 200 contributions to peer-reviewed journals and international conference proceedings. More than 40 articles have appeared in IEEE journals.

Dr. Costa was the Co-Chair of the Technical Program Committee of the European Conference on Antennas and Propagation (EuCAP 2015), Lisbon, and the General Vice-Chair of EuCAP 2017, Paris. He served as an Associate Editor for the IEEE TRANSACTIONS ON ANTENNAS AND PROPAGATION, from 2010 and 2016. He is currently an Associate Editor of the IEEE OPEN JOURNAL OF ANTENNAS AND PROPAGATION. He was a Guest Editor of the IEEE TRANSACTIONS ON ANTENNAS AND PROPAGATION Special Issue on Antennas and Propagation at mm- and submm-Waves in 2013.

CARLOS A. FERNANDES (Senior Member, IEEE) received the Licenciado, M.Sc., and Ph.D. degrees in electrical and computer engineering from the Instituto Superior Técnico (IST), Technical University of Lisbon, Lisbon, Portugal, in 1980, 1985, and 1990, respectively.

In 1980, he joined IST, where he is currently a Full Professor with the Department of Electrical and Computer Engineering in the areas of microwaves, radio wave propagation, and antennas. He is also a Senior Researcher with the Instituto de Telecomunicações and a member of the Board of Directors. He has coauthored a book, two book chapters, and more than 180 technical papers in peer-reviewed international journals and conference proceedings. He holds seven patents in the areas of antennas and radiowave propagation modeling. His current research interests include dielectric antennas for millimeter-wave applications, antennas and propagation modeling for personal communications systems, RFID and UWB antennas, artificial dielectrics, and metamaterials.

Dr. Fernandes was a Guest Editor of the IEEE TRANSACTIONS ON ANTENNAS AND PROPAGATION Special Issue on Antennas and Propagation at mm- and submm-Waves in 2013.